Cavitation as a Mechanism of Substrate Discrimination by Adenylosuccinate Synthetases[†,‡]

Cristina V. Iancu,[§] Yang Zhou, Tudor Borza,[||] Herbert J. Fromm, and Richard B. Honzatko*

Department of Biochemistry, Biophysics, and Molecular Biology, Iowa State University, Ames, Iowa 50011

Received April 18, 2006; Revised Manuscript Received July 14, 2006

ABSTRACT: Adenylosuccinate synthetase catalyzes the first committed step in the de novo biosynthesis of AMP, coupling L-aspartate and IMP to form adenylosuccinate. K_m values of IMP and 2′-deoxy-IMP are nearly identical with each substrate supporting comparable maximal velocities. Nonetheless, the K_m value for L-aspartate and the K_i value for hadacidin (a competitive inhibitor with respect to L-aspartate) are 29−57-fold lower in the presence of IMP than in the presence of 2′-deoxy-IMP. Crystal structures of the synthetase ligated with hadacidin, GDP, and either 6-phosphoryl-IMP or 2′-deoxy-6-phosphoryl-IMP are identical except for the presence of a cavity normally occupied by the 2′-hydroxyl group of IMP. In the presence of 6-phosphoryl-IMP and GDP (hadacidin absent), the L-aspartate pocket can retain its fully ligated conformation, forming hydrogen bonds between the 2′-hydroxyl group of IMP and sequence-invariant residues. In the presence of 2′-deoxy-6-phosphoryl-IMP and GDP, however, the L-aspartate pocket is poorly ordered. The absence of the 2′-hydroxyl group of the deoxyribonucleotide may destabilize binding of the ligand to the L-aspartate pocket by disrupting hydrogen bonds that maintain a favorable protein conformation and by the introduction of a cavity into the fully ligated active site. At an approximate energy cost of 2.2 kcal/mol, the unfavorable thermodynamics of cavity formation may be the major factor in destabilizing ligands at the L-aspartate pocket.

Adenylosuccinate synthetase [IMP, L-aspartate ligase (GDP-forming); EC 6.3.4.4] converts IMP and L-aspartate to adenylosuccinate, using GTP as an energy source. The synthetase participates in de novo purine nucleotide biosynthesis, the purine nucleotide cycle, and salvage pathways for nucleotides (*1*−*3*). Evidence supports a two-step reaction mechanism for adenylosuccinate synthetases. First, the γ-phosphoryl group of GTP is transferred to O-6 of IMP, forming 6-phosphoryl-IMP (6-PIMP).[1] Second, the α-amino group of L-aspartate displaces the 6-phosphoryl group of 6-PIMP to form adenylosuccinate (*1*−*7*). The enzyme adopts a random sequential kinetic mechanism with a strong bias in favor of the association of L-aspartate after the formation of an enzyme·IMP·GTP complex (*8*, *9*).

Bacterial systems have but one form of adenylosuccinate synthetase, but vertebrates have two forms of the enzyme: a basic isozyme, found exclusively in muscle, which is a component of the purine nucleotide cycle and the de novo pathway for the biosynthesis of AMP, and an acidic isozyme, which functions exclusively in de novo AMP biosynthesis (*10*−*15*). The two isoforms in mouse are 75% identical in their amino acid sequences and 40% identical to the enzyme from *Escherichia coli*. AMP is a weak inhibitor of the mouse basic isozyme but a potent inhibitor of the mouse acidic isozyme and the *E. coli* enzyme (*15*). On the other hand, in the presence of saturating levels of IMP, fructose 1,6-bisphosphate is a potent inhibitor of the basic (muscle) isozyme but only a weak inhibitor of the acidic isozyme (*15*). Hence, in heavily exercised muscle, elevated levels of fructose 1,6-bisphosphate could inhibit the basic isozyme, but in other tissues and in bacteria, AMP is the likely regulator of the synthetase.

The de novo synthesis of purine nucleotides in general, and adenylosuccinate synthetase in particular, is the target of numerous natural products that inhibit growth. Hydantocidin, a proherbicide activated specifically in plants, binds only to the active site of adenylosuccinate synthetase (*3*, *16*−*18*). Hadacidin (*N*-formyl-*N*-hydroxyglycine) is an analogue of L-aspartate but inhibits only adenylosuccinate synthetase (*1*−*3*, *19*, *20*). Many cancers (30% of all T-cell acute lymphocytic leukemia, for instance) lack a salvage pathway for adenine nucleotides and rely entirely on de novo biosynthesis of purine nucleotides (*21*). Inhibition of adenylosuccinate synthetase in such tumors would directly decrease the size of the pool of adenine nucleotides, whereas normal cells with intact salvage mechanisms would be impacted to a lesser extent. Allopurinol, an analogue of hypoxanthine, significantly accelerates recovery from complicated malarial infections (*22*). Adenylosuccinate synthetase from *Plasmodium falciparum*, the organism responsible for an estimated 300−500 million annual cases of malaria (*23*,

[†] This work was supported by National Institutes of Health Grant NS 10546.

[‡] Coordinates and structures factors for structures reported here (2GCQ and 2DGN) have been deposited in the Protein Data Bank.

* To whom correspondence should be addressed. Telephone: (515) 294-7103. Fax: (515) 294-0453. E-mail: honzatko@iastate.edu.

[§] Current address: Biology Division, California Institute of Technology, 1200 E. California Blvd., Pasadena, CA 91125.

[||] Current address: Department of Biology, Dalhousie University, Halifax, Nova Scotia B3H 4J1, Canada.

[1] Abbreviations: 6-PIMP, 6-phosphoryl-IMP; 2′-deoxy-6-PIMP, 2′-deoxy-6-phosphoryl-IMP.

10.1021/bi0607498 CCC: $33.50
Published on Web 09/02/2006

24), assimilates allopurinol ribonucleotide into pathways that ultimately poison ribosomal translation (*25*, *26*). A clear understanding of substrate recognition in adenylosuccinate synthetase could facilitate the development of tight-binding inhibitors and substrate analogues that impair purine nucleotide biosynthesis and cell growth.

In the case of inhibition by hydantocidin and hadacidin, the inhibitor molecule combines with other ligands to fill the active site of the synthetase. Hydantocidn is phosphosphorylated on its 5′-hydroxyl group to make an analogue of IMP that binds synergistically with P_i and GDP (*16*−*18*). Hadacidin coordinates the active site Mg^{2+} with its *N*-formyl group and packs against the base moiety of IMP (*5*−*7*, *27*). The structural feature common to hadacidin and hydantocidin complexes of adenylosuccinate synthetase is a set of ligands that interact well with the protein and with each other. Interactions between ligands and protein and between ligands determine the stability of the complex.

The exacting fit of substrates and substrate analogues in inhibited complexes of adenylosuccinate synthetase, then, was difficult to reconcile with a report identifying 2′-deoxy-IMP as an effective substrate of adenylosuccinate synthetase (*28*). The 2′-hydroxyl group of IMP interacts with the side chain of a sequence-conserved arginine and with the backbone carbonyl of a sequence-conserved valine. How could the loss of this hydroxyl group have little or no effect on the stability of the substrate complex?

Here we report a role for the 2′-hydroxyl group of IMP in the recognition of L-aspartate. Indeed, as indicated by the earlier study (*28*), recombinant synthetases from *E. coli* and mouse muscle have similar K_m values for 2′-deoxy-IMP and IMP. Both enzymes, however, exhibit 29−57-fold increases in their K_m values for L-aspartate ($K_m^{L-aspartate}$) and K_i values for hadacidin ($K_i^{hadacidin}$) when 2′-deoxy-IMP replaces IMP. Crystal structures of the *E. coli* synthetase, having bound GDP, hadacidin, and either 6-PIMP or 2′-deoxy-6-PIMP, reveal no conformational differences within experimental uncertainty; the absence of the 2′-hydroxyl group introduces only a cavity. On the other hand, crystalline complexes of the mouse muscle synthetase without hadacidin, but having bound GDP and either 6-PIMP or 2′-deoxy-6-PIMP, differ significantly. Disorder in the L-aspartate pocket is correlated with the loss of hydrogen bonds normally associated with the 2′-hydroxyl group of IMP. Although disorder in the L-aspartate pocket may contribute to increases in $K_i^{hadacidin}$ and $K_m^{L-aspartate}$, cavity formation in the fully ligated enzyme by itself can account for the observed increases in kinetic parameters. The packing efficiency of ligands in the active site of a multisubstrate enzyme can be a significant determinant in substrate recognition and an important consideration in screening for tight-binding inhibitors.

EXPERIMENTAL PROCEDURES

Materials. All reagents, including GTP, IMP, L-aspartate, bovine serum albumin, and DEAE-Sepharose, were from Sigma unless noted otherwise. Hadacidin was a generous gift from F. Rudolph and B. Cooper (Department of Biochemistry and Cell Biology, Rice University, Houston, TX). Plasmids for the expression of the enzyme are those employed in previous investigations (*15*, *29*).

Expression and Purification of Mouse Muscle and E. coli Adenylosuccinate Synthetase. The recombinant *E. coli* and mouse basic isozyme were prepared as described previously (*29*, *30*). Enzyme purity was assayed by sodium dodecyl sulfate−polyacrylamide gel electrophoresis (SDS−PAGE). Investigations here employed the mouse muscle isozyme with its N-terminal polyhistidyl tag in place. The presence of the polyhistidyl tag has no effect on the kinetics of the mouse basic isozyme (*30*); however, only the tagged form of protein has been crystallized (*27*, *30*, *31*). Recombinant *E. coli* adenylosuccinate synthetase used here does not have an affinity tag (*29*).

Enzyme Assays. Protein concentrations were determined by the method of Bradford (*32*), using bovine serum albumin as a standard. Enzyme activity was determined by the change in absorbance at 290 nm and at 22 °C as described previously (*8*). Using up to 1 μg/mL enzyme (22 nM subunit concentration), the reaction was linear for at least 1 min. K_m and V_{max} values for each substrate were obtained by holding the other two substrates at saturating levels (100 μM GTP, 300 μM IMP or 2′-deoxy-IMP, and 2 mM L-aspartate with IMP or 200 mM L-aspartate with 2′-deoxy-IMP) and varying the concentration of the third substrate. In the determination of K_m values, initial concentrations of GTP varied systematically from 5 to 100 μM, those of IMP (or 2′-deoxy-IMP) from 25 to 300 μM, and those of L-aspartate from 0.1 to 2 mM (for IMP) or from 1 to 96 mM (for 2′-deoxy-IMP). In the determination of K_i values of hadacidin, concentrations of GTP and IMP were maintained at saturating levels (100 and 300 μM, respectively) as initial concentrations of L-aspartate and hadacidin varied from 0.125 to 2 mM and from 0.25 to 16 μM, respectively. K_i values of hadacidin in the presence of 2′-deoxy-IMP employed fixed initial concentrations of GTP and 2′-deoxy-IMP of 100 and 300 μM, respectively, as initial concentrations of L-aspartate and hadacidin varied from 4 to 64 mM and from 10 to 160 μM, respectively. For the *E. coli* enzyme, the assay buffer contained 20 mM Hepes (pH 7.7) and 6 mM magnesium chloride and, for the mouse enzyme, 20 mM Hepes (pH 7.2) and 8 mM magnesium acetate. All data were analyzed with GraFit (*33*). Models for competitive, noncompetitive, uncompetitive and mixed inhibition were fit to hadacidin inhibition data.

Crystallization. Crystals were grown by the method of hanging drops. The mouse muscle enzyme crystallized from equal parts of a protein solution [10 mg/mL protein in 50 mM Hepes (pH 7.5), 50 mM NaCl, 1 mM dithiothreitol (DTT), 0.5 mM EDTA, 10 mM GTP, and 10 mM 2′-deoxy-IMP] and a precipitant solution [100 mM Hepes (pH 7.0), 200 mM magnesium acetate, and 12−14% (w/v) polyethylene glycol 8000 or 12−17% (w/v) polyethylene glycol 3350]. Crystals of the *E. coli* enzyme grew from equal parts of a protein solution [10 mg/mL protein in 50 mM Hepes (pH 7.0), 50 mM NaCl, 1 mM dithiothreitol (DTT), 0.5 mM EDTA, 5 mM GTP, 5 mM 2′-deoxy-IMP, 2 mM hadacidin, and 10 mM magnesium acetate] and a precipitant solution [100 mM Hepes (pH 7.0), 200 mM magnesium acetate, and 12−16% (w/v) polyethylene glycol 8000]. In all experiments, droplet volumes were 6 μL and wells contained 500 μL of the precipitant solution. Equal dimensional prisms of 100 μm appeared within 3 days at 22 °C. Crystals of the *E. coli* and mouse muscle enzymes were transferred to a solution of 50 mM Hepes (pH 7.0), 100 mM magnesium acetate, 27% (w/v) polyethylene glycol 8000, and 21% (v/v) glycerol and then frozen in liquid nitrogen.

Table 1: Kinetic Parameters for Recombinant Adenylosuccinate Synthetases from *E. coli* and Mouse Muscle Using IMP and 2′-Deoxy-IMP[a]

	E. coli	mouse muscle
IMP reaction		
k_{cat} (s^{-1})	1.00 ± 0.05	5.4 ± 0.4[b]
K_m^{IMP} (μM)	28 ± 1	45 ± 7[b]
K_m^{GTP} (μM)	26 ± 2	12 ± 2[b]
$K_m^{L-aspartate}$ (μM)	230 ± 40	140 ± 20[b]
$K_i^{hadacidin}$ (μM)	0.49 ± 0.08	0.32 ± 0.05
2′-deoxy-IMP reaction		
k_{cat} (s^{-1})	0.96 ± 0.05	5.5 ± 0.2
$K_m^{2'-deoxy-IMP}$ (μM)	41 ± 4	58 ± 8
K_m^{GTP} (μM)	21 ± 1	15 ± 2
$K_m^{L-aspartate}$ (mM)	13 ± 5	4 ± 0.2
$K_i^{hadacidin}$ (μM)	17 ± 3	14 ± 3

[a] Conditions of the assay are in Experimental Procedures. [b] From ref *15*.

Data Collection, Model Building, and Refinement. Data for the mouse muscle complex were collected at beamline 9-2 of the Stanford Synchrotron Radiation Laboratory, using an ADSC Quantum 4 CCD detector. The wavelength of radiation was 0.979 Å, and the temperature of data collection was 120 K. Data reduction employed Denzo/Scalepack (*34*). Data for the *E. coli* complex were collected at Iowa State University on a Rigaku R-AXIS IV^{++} image plate detector using an Osmic confocal mirror system (Cu Kα radiation) and a sample temperature of 100 K. Data reduction employed CrystalClear (*35*). Intensities were converted to structure factors using the CCP4 program TRUNCATE (*36*). Structures were determined by molecular replacement, using AmoRe (*37*) and models for the fully ligated mouse muscle enzyme [Protein Data Bank entry 1LON (*27*)] and the *E. coli* enzyme [Protein Data Bank entry 1CGO (*7*)]. Model building and refinement employed XTALVIEW (*38*) and CNS (*39*), respectively. Force constants and parameters of stereochemistry were from Engh and Huber (*40*). Criteria for the addition of water molecules were identical to those of previous studies (*5*−*7*). Estimates of coordinate error used the method of Luzzati (*41*). Evaluation of the stereochemistry of the refined model employed PROCHECK (*42*). Superposition of structures employed software from the CCP4 package (*43*) or XTALVIEW (*38*).

Estimates of Cavitation Energies. The contribution to the total potential energy of the 2′-hydroxyl group of 6-PIMP in the fully ligated complexes of the *E. coli* and mouse muscle synthetases was calculated using AutoDock 3.0 (*44*). van der Waals interactions between the 2′-O atom and atoms within a sphere with a radius of 10 Å were identified. The calculation sums pairwise interaction energies between the 2′-O atom of 6-PIMP and the approximately 200 carbon, nitrogen, and oxygen atoms within a limiting distance (10 Å) of the 2′-O atom. The interaction energies are based on a Lennard-Jones 6−12 function, using parameters in AutoDock 3.0. Parameters are not available for interactions involving Mg^{2+}; however, as Mg^{2+} is approximately 9.8 Å from the 2′-hydroxyl group of 6-PIMP in synthetase structures, the contribution of a single Mg^{2+}−O contact to the total energy is negligible.

Table 2: Statistics of Data Collection and Refinement

	E. coli GDP·2′-deoxy-6-PIMP·hadacidin complex	mouse muscle GDP·2′-deoxy-6-PIMP complex
space group	$P3_221$	$P4_32_12$
unit cell parameters		
a (Å)	80.59	70.11
b (Å)	80.59	70.11
c (Å)	158.5	199.0
resolution limits (Å)	25−2.0	16−2.4
no. of reflections collected	285758	244020
no. of unique reflections	39551	20371
completeness of data (%) (overall/last shell)[a]	96.4/78.5	98.9/98.9
R_{merge}[b] (overall/last shell)[a]	0.055/0.265	0.100/0.415
no. of reflections in refinement[c]	39498	19121
no. of atoms	3384	3408
no. of solvent sites	169	128
R/R_{free}[d]	0.224/0.251	0.198/0.262
mean *B* value (Å^2)		
protein	38	35
ligands	36	27
root-mean-square deviation		
bond lengths (Å)	0.006	0.006
bond angles (deg)	1.3	1.2
dihedral angles (deg)	23	23
improper dihedral angles (deg)	0.83	0.85

[a] The resolution range for the last shell is 2.0−2.07 Å for the *E. coli* complex and 2.4−2.5 Å for the mouse muscle complex. [b] $R_{merge} = \sum_j\sum_i|I_{ij} - \langle I_j\rangle|/\sum_i\sum_j I_{ij}$, where *i* runs over multiple observations of the same intensity and *j* runs over crystallographically unique intensities. [c] All data for which $|F_{obs}| > 0$. [d] *R* factor $= \sum||F_{obs}| - |F_{calc}||/\sum|F_{obs}|$, where $|F_{obs}| > 0$.

RESULTS

Enzyme Purity and Kinetics. Proteins used in assays and crystallization were at least 95% pure on the basis of sodium dodecyl sulfate−polyacrylamide gel electrophoresis (SDS−PAGE). 2′-Deoxy-IMP is a substrate of the synthetase (*28*), but prior to the study presented here, no information was available regarding the kinetics of an adenylosuccinate synthetase reaction supported by 2′-deoxy-IMP. K_m values for 2′-deoxy-IMP and IMP (Table 1) for both the *E. coli* and mouse muscle enzyme are equal within experimental uncertainty. All other parameters are equivalent for the two reactions except those associated with L-aspartate and hadacidin. $K_m^{L-aspartate}$ increases 57- and 29-fold and $K_i^{hadacidin}$ 35- and 44-fold for *E. coli* and mouse muscle enzymes, respectively, in reactions that use 2′-deoxy-IMP instead of IMP. Evidently, the *E. coli* and mouse muscle adenylosuccinate synthetases, broadly representative of microbial and vertebrate systems, have a mechanism for distinguishing ribonucleotide and 2′-deoxyribonucleotide substrates. That mechanism is indirect; the recognition of the nucleotide itself is equally robust, but in some way, the 2′-hydroxyl group of the ribonucleotide is an essential determinant in the recognition of L-aspartate and for high-affinity binding of hadacidin.

Existing Crystal Structures of Ribonucleotide Complexes of E. coli and Mouse Muscle Synthetases. Crystal structures of synthetases from *E. coli* and mouse muscle exist in ligand-free and fully ligated complexes (*7*, *27*, *30*). For the latter, GDP, 6-PIMP, hadacidin (as an analogue of L-aspartate), and Mg^{2+} are in the active site. In addition, a structure is available for the 6-PIMP·GDP complex for the mouse muscle enzyme (*27*) and for the Arg303 → Leu *E. coli* enzyme, which has a low affinity for hadacidin and a high K_m for L-aspartate (*7*, *45*). In fully ligated complexes, the 2′-hydroxyl group of IMP hydrogen bonds with a backbone carbonyl group of a peptide link between sequence-invariant residues (Val273 and Gly274 in the *E. coli* synthetase and Val305 and Gly306 in the mouse muscle enzyme). The 2′-hydroxyl group also hydrogen bonds with an arginyl side chain (Arg303 and Arg335 in the *E. coli* and mouse muscle enzymes, respectively). Arg303 (and probably the corresponding position in the mouse muscle isozyme, Arg335) is essential for the recognition of L-aspartate, as its mutation to leucine causes a 200-fold increase in the K_m for L-aspartate (*45*). Hadacidin makes only nonbonded contacts with 6-PIMP in fully ligated complexes.

Fully Ligated 2′-Deoxyribonucleotide Complex of the E. coli Synthetase (Protein Data Bank entry 2GCQ). Statistics of data collection and refinement for crystals of the *E. coli* synthetase grown in 2′-deoxy-IMP, GTP, hadacidin, and Mg^{2+} are listed in Table 2. The active site contains a single Mg^{2+} to which are coordinated 2′-deoxy-6-PIMP, GDP, and hadacidin (Figure 1). Electron density associated with 2′-deoxy-6-PIMP is strong, but no observable density is associated with what would be the position of a 2′-hydroxyl group (Figure 2). Interactions between active site ligands and the protein are identical to those of the 6-PIMP, GDP, hadacidin, and Mg^{2+} complex (PDB entry 1CGO) (Figure 3). Specifically, as the focus here is on the binding of hadacidin, the oxygen atom of its *N*-formyl group coordinates Mg^{2+}, its *N*-hydroxyl group hydrogen bonds with Asp13,

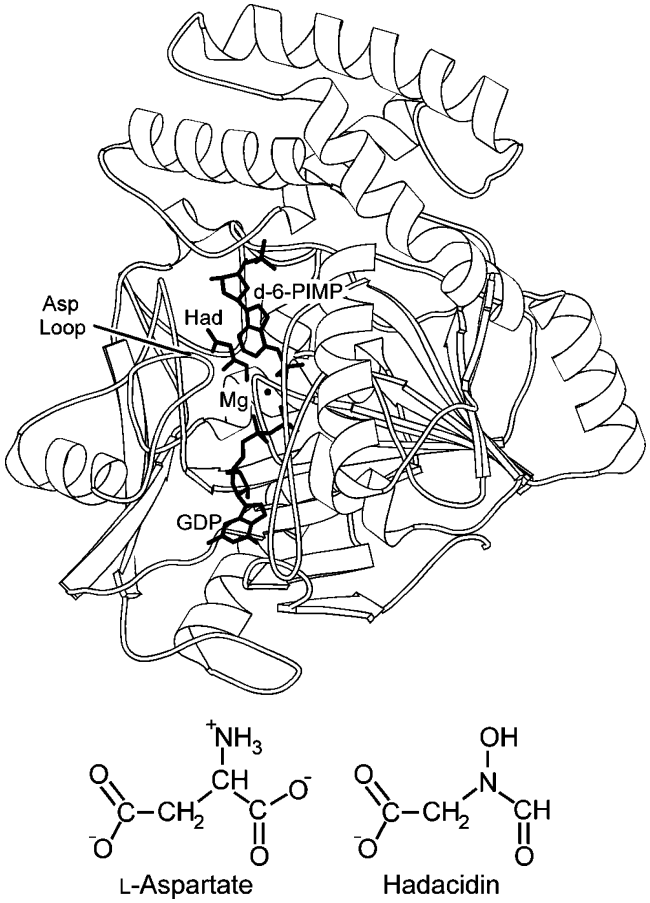

FIGURE 1: Overview of the 2′-deoxy-6-PIMP·GDP·hadacidin·Mg^{2+} complex. Shown is a single subunit of the *E. coli* dimer with bound ligands defining the viewing orientation of Figures 2−6 (top). The labels Had and d-6-PIMP represent hadacidin and 2′-deoxy-6-PIMP, respectively. Structures of L-aspartate and hadacidin are compared (bottom). This figure was drawn with MOLSCRIPT (*57*).

and its β-carboxyl group hydrogen bonds with Thr301, Arg303, and the backbone amide groups of Thr300 and Thr301 (Figure 4). The aforementioned distances in the 6-PIMP and 2′-deoxy-6-PIMP complexes exhibit a root-mean-square deviation of 0.22 Å, well within the estimated uncertainty in coordinates of 0.25 Å, and no distance between corresponding atoms in the two complexes exceeds 0.4 Å. In fact, the principal difference in the fully ligated *E. coli* structures is the void left by the absence of the 2′-hydroxyl group in the 2′-deoxy-IMP complex.

Partially Ligated 2′-Deoxyribonucleotide Complex of the Mouse Muscle Synthetase (Protein Data Bank entry 2DGN). Statistics of data collection and refinement appear in Table 2 for the mouse basic enzyme crystallized with 2′-deoxy-IMP, GTP, and Mg^{2+}. The active site contains a single Mg^{2+} that coordinates 2′-deoxy-6-PIMP and GDP. Electron density associated with the ligands is strong, but no density is present at what would be the position of the 2′-hydroxyl group.

Unlike the fully ligated structures of the *E. coli* and mouse muscle enzymes, the partially ligated complexes of the mouse basic isozyme exhibit significant conformational differences in their L-aspartate binding pockets (Figure 5). The mouse muscle enzyme with 6-PIMP, GDP, and Mg^{2+} (Protein Data Bank entry 1LNY) has a dimer in the asymmetric unit. Backbone carbonyl groups of residues 332−334 of chain B hydrogen bond in a lattice contact that stabilizes the aspartate

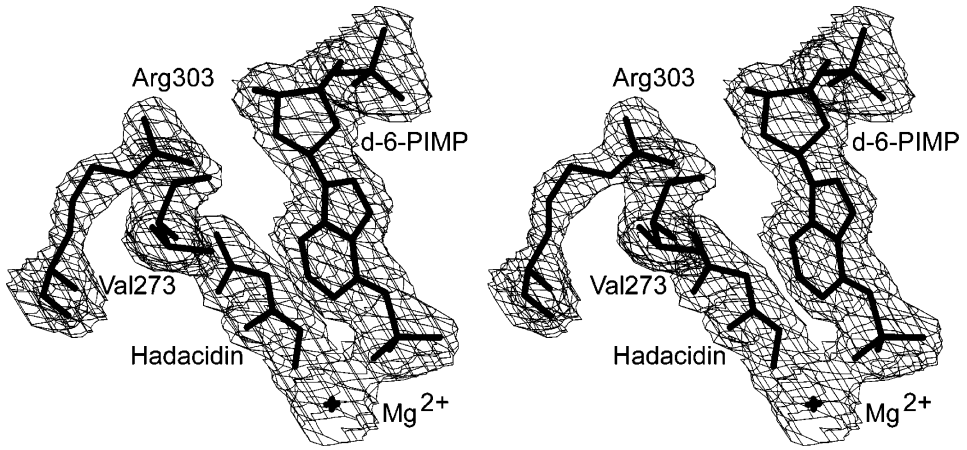

FIGURE 2: Stereoview of 2′-deoxy-6-PIMP with electron density in the fully ligated complex of the *E. coli* synthetase. The electron density is from an omit map (in which atoms for 2′-deoxy-6-PIMP have been omitted in the calculation of phase angles) with a contour level of 1.5σ and a cutoff radius of 1.5 Å. The label d-6-PIMP represents 2′-deoxy-6-PIMP.

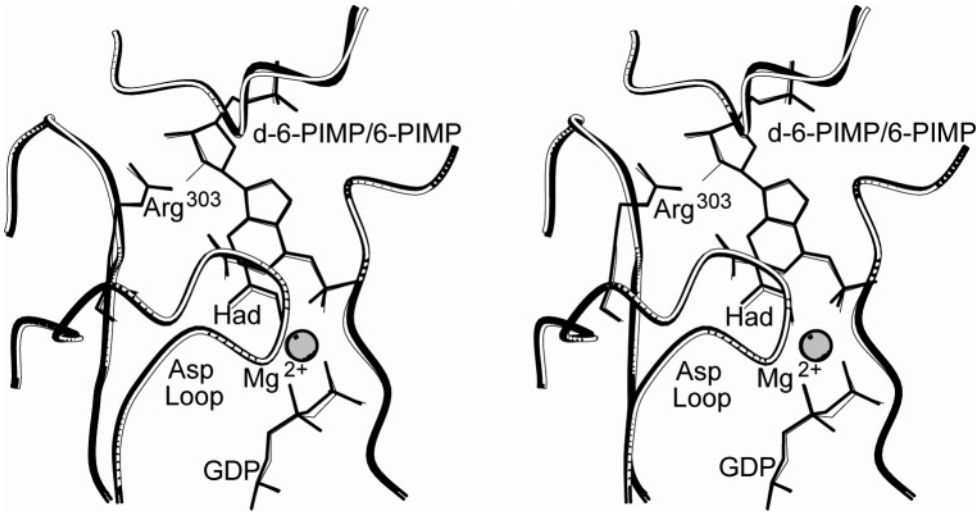

FIGURE 3: Stereoview of superpositions of fully ligated complexes of *E. coli* adenylosuccinate synthetase. The complex of 6-PIMP, GDP, hadacidin, and Mg^{2+} (white with thin lines) nearly overlays that of 2′-deoxy-6-PIMP, GDP, hadacidin, and Mg^{2+} (black with thick lines). The labels Had and d-6-PIMP represent hadacidin and 2′-deoxy-6-PIMP, respectively. Superpositions are based on Cα alignments of Figure 2 of ref *30*. This figure was drawn with MOLSCRIPT (*57*).

binding loop (residues 330−336) some 5 Å from its position in fully ligated structures of the mouse muscle and *E. coli* enzymes (*7*, *27*). Distances from Thr332 OG1 to Asn68 O and Gly70 N are 9.46 and 9.95 Å, respectively, ∼6.2 Å longer than the corresponding distances in the fully ligated mouse muscle enzyme. Arg335 (equivalent to Arg303 in the *E. coli* synthetase) and the backbone carbonyl group of Val305 (corresponding to Val273 of the *E. coli* enzyme) do not hydrogen bond with the 2′-hydroxyl group of the ribonucleotide in chain B. The aspartate loop of chain A participates in a different set of lattice contacts involving backbone carbonyl groups of residues 333 and 334, as well as a side chain stacking interaction involving Trp329. Nonetheless, the conformation of the aspartate loop in chain A is similar to that of the fully ligated structure. Specifically, Arg335 and the backbone carbonyl of Val305 hydrogen bond with the 2′-hydroxyl group of IMP, as observed in fully ligated systems. Distances in chain A from Thr332 OG1 to Asn68 O and Gly70 N are 6.81 and 6.77 Å, respectively, ∼3.5 Å longer than those in the fully ligated mouse muscle enzyme.

In contrast to the 6-PIMP·GDP·Mg^{2+} complex, the asymmetric unit of the 2′-deoxy-6-PIMP·GDP·Mg^{2+} mouse muscle complex has but a single subunit. The enzyme is still a dimer; however, its axis of molecular symmetry coincides with a crystallographic axis of 2-fold symmetry. The 6-PIMP·GDP·Mg^{2+} and 2′-deoxy-6-PIMP·GDP·Mg^{2+} complexes have nearly equivalent structures (root-mean-square deviation for superimposed Cα atoms of 0.4 Å) except for their aspartate loops. Interactions involving Arg335 and the backbone carbonyl of Val305 are absent as expected. Moreover, the aspartate loop is withdrawn from the active site: distances from Thr332 OG1 to Asn68 O and Gly70 N are 9.46 and 9.85 Å, respectively (Figure 4). The conformation of the aspartate loop in the 2′-deoxy-6-PIMP·GDP·Mg^{2+} complex is much like that of the aspartate loop in chain B of the 6-PIMP·GDP·Mg^{2+} structure, but the outwardly displaced loop cannot be attributed to a lattice contact.

Energy Differences in 6-PIMP and 2′-Deoxy-6-PIMP Complexes. The crystal structures of the fully ligated complexes 6-PIMP and 2′-deoxy-6-PIMP of the *E. coli* synthetase are identical within experimental error. Hence, the energy of interaction involving the 2′-hydroxyl group in the fully ligated 6-PIMP complex is an estimate of the energy penalty due to the absence of that group. As fully ligated 6-PIMP complexes are available for the *E. coli* and mouse

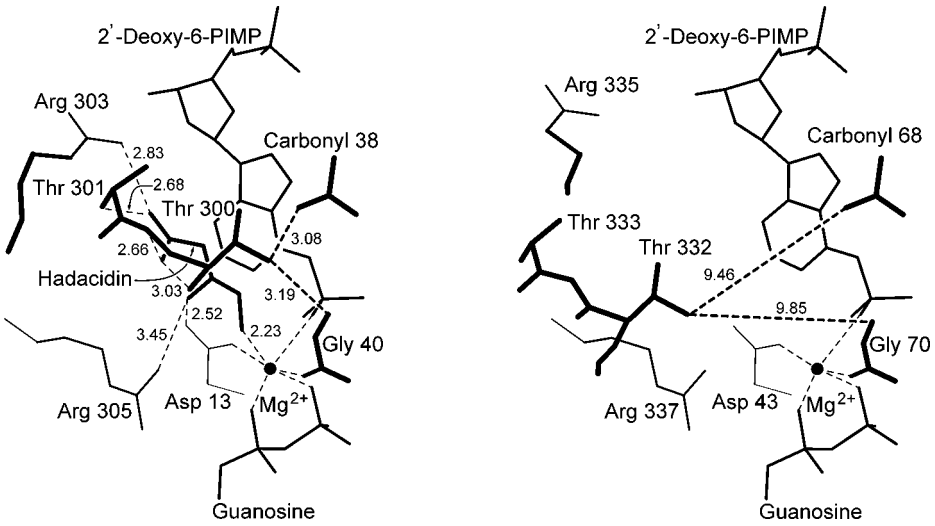

FIGURE 4: Schematic of the aspartyl pocket of adenylosuccinate synthetase. Distances (in angstroms) in the 2′-deoxy-6-PIMP·GDP·hadacidin (fully ligated) complex and the 2′-deoxy-6-PIMP·GDP (partially ligated) complex are shown in the left and right panels, respectively. Distances from Thr300 OG1 to carbonyl 38 and amide 40 (corresponding to distances from Thr332 OG1 to carbonyl 68 and amide 70 in the mouse enzyme) provide a measure of the movement of the Asp loop (see Figure 1 for a definition) relative to the active site.

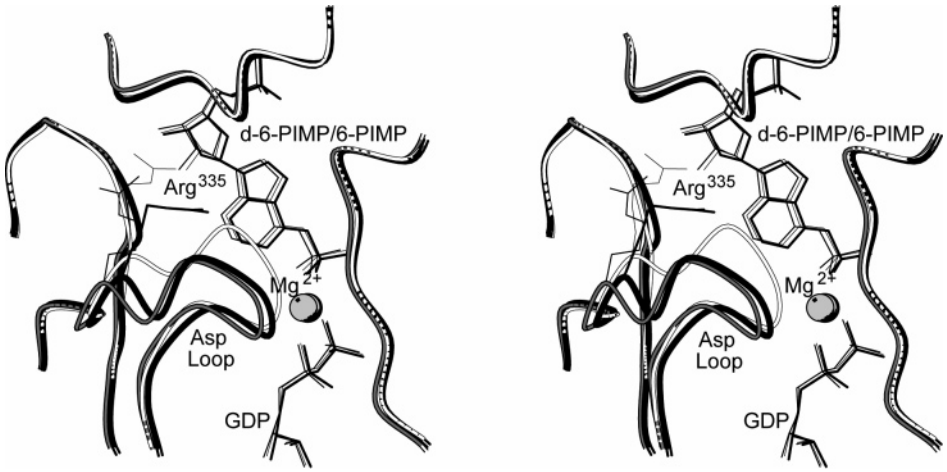

FIGURE 5: Stereoview of superpositions of partially ligated complexes of mouse muscle adenylosuccinate synthetase. Complexes of 6-PIMP, GDP, and Mg^{2+} (chain A, white with thin lines, and chain B, gray with medium lines) are superimposed on the complex of 2′-deoxy-6-PIMP (black with thick lines). The label d-6-PIMP represents 2′-deoxy-6-PIMP. Superpositions are based on Cα alignments of Figure 2 of ref *30*. This figure was drawn with MOLSCRIPT (*57*).

Table 3: Interaction Energies Involving the 2′-Hydroxyl Group of 6-PIMP in Fully Ligated Complexes of *E. coli* and Mouse Muscle Adenylosuccinate Synthetase

interacting atoms	no. of interactions	energy (kcal/mol)
E. coli		
O2′−C	107	−1.487
O2′−N	45	−0.371
O2′−O	50	−0.481
total	202	−2.339
mouse muscle		
O2′−C	108	−1.247
O2′−N	47	−0.481
O2′−O	44	−0.463
total	199	−2.190

muscle synthetases (PDB entries 1CG0 and 1LON, respectively), the interaction energies can be calculated for both systems. The interaction energies of the 2′-hydroxyl groups in the *E. coli* and mouse muscle systems from AutoDock 3.0 (Table 3) are nearly identical, in harmony with the nearly identical sequences and structures of the two complexes in the region that is being considered (*27*).

DISCUSSION

The kinetic mechanism for the *E. coli* enzyme is rapid-equilibrium random (*8*, *9*). Hence, $K_m^{L-aspartate}$ is a reasonable approximation of the equilibrium constant governing the dissociation of L-aspartate from the enzyme·IMP·GTP·L-aspartate·Mg^{2+} complex. Moreover, changes in $K_i^{hadacidin}$ are consistent with those in $K_m^{L-aspartate}$, further evidence of rapid equilibrium kinetics. L-Aspartate and hadacidin then dissociate more readily from the 2′-deoxy-IMP complex than from the IMP complex, and this is true to the same extent for the *E. coli* and mouse muscle enzymes.

A factor in the relatively weak association of L-aspartate and hadacidin in the presence of 2′-deoxy-IMP is the loss of hydrogen bonds involving the side chain of a conserved arginine (positions 303 and 335 in *E. coli* and mouse muscle enzymes, respectively) and the backbone carbonyl group of a conserved valine (positions 273 and 305 in *E. coli* and mouse muscle enzymes, respectively). Complexes of 6-PIMP, GDP, and Mg^{2+} of the mouse muscle enzyme (Protein Data Bank entry 1LNY, space group *C*2) indicate a predisposition

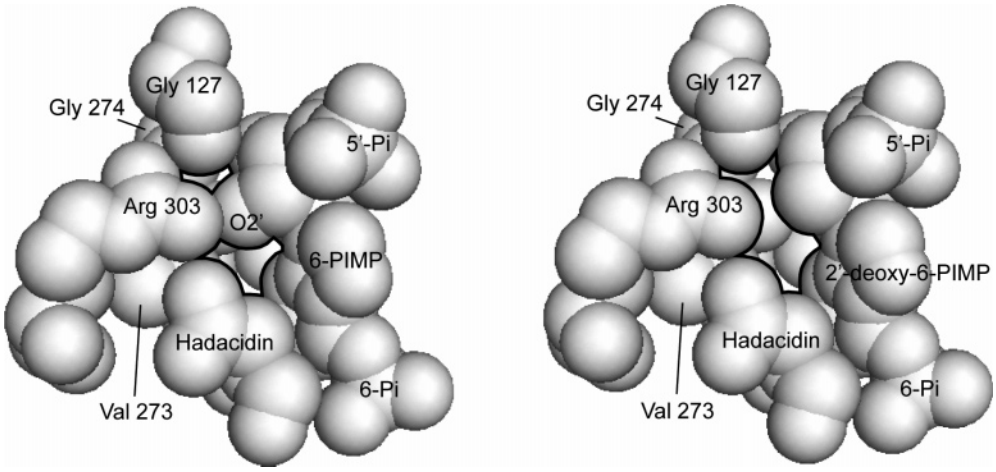

FIGURE 6: Space filling models of the fully ligated complex of the *E. coli* synthetase. Packing voids in the vicinity of the 2′-hydroxy group of 6-PIMP (left) and in its absence in the 2′-deoxy-6-PIMP complex (right) are indicated by dark outlines of the atoms determining the void. This figure was drawn with PyMOL (*58*).

to form hydrogen bonds involving the 2′-hydroxyl group of 6-PIMP even in the absence of hadacidin. When these hydrogen bonds are intact (as in chain A of 1LNY), the L-aspartate loop assumes a conformation much like that of the fully ligated complexes of the synthetase. Lattice contacts observed in the mouse muscle crystal structure (1LNY), however, introduce an element of uncertainty. We do not know whether hydrogen bonds involving the 2′-hydroxyl of 6-PIMP form in solution in the absence of L-aspartate. If such hydrogen bonds do form, they have no influence on the K_m of IMP, and hence, the free energy from such interactions must go toward stabilizing a subset of conformations favorable for the binding of L-aspartate.

A more intriguing contribution to the elevated kinetic parameters for L-aspartate and hadacidin is the cavity that replaces the 2′-hydroxyl group of the fully ligated 2′-deoxyribonucleotide complex. Water does not occupy the site left vacant by the absent 2′-hydroxyl group, and the protein structure does not relax to fill the void. Hence, the cost of cavity formation to a first approximation is the loss of all interactions involving the 2′-hyroxyl group in the fully ligated complex. Assuming the entropy is not changed significantly in a thermodynamic transition from a 6-PIMP to a 2′-deoxy-6-PIMP complex, the calculated difference in potential energy is a fair approximation of the free energy differences in the ribonucleotide and deoxyribonucleotide complexes. The energy difference ranges from 2.2 to 2.3 kcal/mol, which would increase dissociation constants for hadacidin by 41−49-fold. The calculated increases are close to those of observed kinetic parameters and suggest that cavity formation is the primary cause of the observed behavior.

Curiously, the absence of the 2′-hydoxyl group influences only kinetic parameters of hadacidin and L-aspartate. One would expect an increase in the K_m of 2′-deoxy-IMP relative to that of IMP, as the loss in hydrogen bonding potential and nonbonded interactions are due to the absence of a functional group covalently attached to the nucleotide. An explanation of this phenomenon may rest with the kinetic mechanism of the synthetase. Although that mechanism is random, isotope exchange kinetics indicate that in 90% of synthetase turnovers L-aspartate is the last substrate to bind to the enzyme (*9*). Evidently, when IMP binds to the active site, its base encroaches upon the L-aspartate pocket (*27*). Phosphorylation at the 6-position of IMP introduces numerous interactions that "bend" the purine base away from the L-aspartate pocket (*31*). Hence, the formation of 6-PIMP removes steric barriers to the productive binding of L-aspartate. As the cavity due to the absent 2′-hydroxyl group does not exist until L-aspartate binds (and for the vast majority of turnovers, binds last of the three substrates), the negative impact of cavity formation is felt entirely by the amino acid substrate.

The unfavorable free energy of cavity formation may be a factor in the weak binding of small amino acids (glycine, alanine, and serine) to the synthetase[2] and may account for the relatively weak inhibition of adenylosuccinate synthetases by succinate. Succinate has the carboxyl groups of L-aspartate but lacks the steric encumbrance of an α-amino group, yet $K_m^{L-aspartate}$ is 4-fold lower than the $K_i^{succinate}$ for the *E. coli* enzyme (*46*). If, however, the succinate complex of the synthetase leaves a void where an α-amino group should be, its K_i would be high relative to the K_m of L-aspartate.

Cavity formation as a means of discriminating substrates is not unprecedented. In fact, the selection of the correct amino acid by aminoacyl-tRNA synthetases is due at least in part to the penalty of placing a hydrogen atom in a binding pocket designed for a larger functional group. L-Valine suffers an approximately 3.4 kcal/mol penalty relative to L-isoleucine in binding to the recognition pocket of isoleucyl-tRNA synthetase, and a penalty of similar magnitude occurs in the binding of L-α-aminobutyric acid to valyl-tRNA synthetase (*47*−*49*). Energy shortfalls for the association of L-alanine with cysteinyl-tRNA synthetase and L-phenylalanine to tyrosyl-tRNA synthetase are even greater (9.1 and 7.0 kcal/mol, respectively) and result in effective substrate discrimination without recourse to editing mechanisms (*49*, *50*). The high energy penalties of tRNA synthetases, attributed to the loss of interactions of a missing carbon, oxygen, or sulfur atom, infer a rigid pocket for the amino acid side chain, surrounded by densely packed protein atoms. By comparison, the energy penalty caused by 2′-deoxy-IMP (2.2−2.3 kcal/mol) is relatively modest, and clearly, one

[2] Aaron ver Heul and Richard B. Honzatko, unpublished observations.

observes "empty space" in the vicinity of the 2′-hydroxy group even for the correct substrate (Figure 6).

Purine nucleoside phosphorylase should maintain low concentrations of 2′-deoxyinosine so that for normal mammalian cell types, concentrations of 2′-deoxy-IMP should be low relative to those of IMP. The relatively high K_m for L-aspartate in the presence of 2′-deoxy-IMP further assures that the de novo pathway would not be a source of 2′-deoxy-AMP. Certain melanomas, however, lack purine nucleoside phosphorylase, and in such cell types, 2′-deoxyinosine may become phosphorylated and enter the de novo purine nucleotide pathway (*51*). Adenylosuccinate synthetase discriminates against 2′-deoxy-IMP as a substrate, but IMP dehydrogenase reportedly does not distinguish between 2′-deoxy-IMP and IMP (*52*). Hence, at the very least, an increase in the ratio of 2′-deoxy-IMP to IMP should lead to an increase in levels of 2′-deoxy-GTP. An increase in the level of 2′-deoxy-GTP (a substrate for adenylosuccinate synthetase) could offset reduced flux through adenylosuccinate synthetase due to the inhibitory effects of 2′-deoxy-IMP. Indeed, Musk et al. (*51*) report 25- and 11-fold increases in the levels of 2′-deoxy-GTP and 2′-deoxy-ATP, respectively, in a melanoma (MM96L cell line) deficient in purine nucleoside phosphorylase. Increased levels of 2′-deoxypurine nucleotides in melanomas may be responsible for base misincorporation and the emergence of a mutator phenotype that causes the progressive transformation of the melanoma (*51*).

Other multisubstrate enzymes exhibit substrate-linked substrate recognition phenomena. Pantothenate synthetase from *Mycobacterium tuberculosis* must synthesize the pantoyl adenylate intermediate before it can bind β-alanine (*53*, *54*). The phosphoryl group of the pantoyl adenylate intermediate hydrogen bonds with the amino group of β-alanine, positioning that group for its nucleophilic attack on the carbonyl carbon of the intermediate (*54*). The amino group of glycinamide ribonucleotide (GAR) may play a critical role in the binding of formate to the active site of glycinanide ribonucleotide transformylase (*55*), and evidently, the affinity of *Hha*I DNA methyltransferase for DNA is enhanced some 900-fold in the presence of its cofactor *S*-adenosyl-L-methionine (*56*). The mutual recognition of substrates in the active site may be a general phenomenon in multisubstrate systems, and in such systems, an unchanged K_m for a substrate alternative does not ensure the proper recognition of other components of the assembled enzyme−substrate complex.

Cavity formation is a significant consideration in the design of tight-binding inhibitors. In the case of adenylosuccinate synthetase and perhaps for other multisubstrate systems, it may be possible to design or discover "complementary" inhibitors, molecules that by themselves inhibit weakly but when combined with other ligands result in potent inhibition. In fact, hydantocidin owes its potent inhibition ($K_i \sim 20$ nM) of adenylosuccinate synthetase to its tight packing with phosphate and GDP in the active site (*18*). A screen of adenylosuccinate synthetase in its complex with 2′-deoxy-6-PIMP and GDP or fructose 1,6-bisphosphate and GDP could lead to tight-binding alternatives to hadacidin.

REFERENCES

1. Stayton, M. M., Rudolph, F. B., and Fromm, H. J. (1983) Regulation, genetics, and properties of adenylosuccinate synthetase: A review, *Curr. Top. Cell. Regul. 22*, 103−141.
2. Honzatko, R. B., and Fromm, H. J. (1999) Structure-function studies of adenylosuccinate synthetase from *Escherichia coli*, *Arch. Biochem. Biophys. 370*, 1−8.
3. Honzatko, R. B., Stayton, M. M., and Fromm, H. J. (1999) Adenylosuccinate synthetase: Recent developments, *Adv. Enzymol. Relat. Areas Mol. Biol. 73*, 57−102.
4. Bass, M. B., Fromm, H. J., and Rudolph, F. B. (1984) The mechanism of the adenylosuccinate synthetase reaction as studied by positional isotope exchange, *J. Biol. Chem. 259*, 12330−12333.
5. Poland, B. W., Fromm, H. J., and Honzatko, R. B. (1996) Crystal structures of adenylosuccinate synthetase from *Escherichia coli* complexed with GDP, IMP hadacidin, NO^{3-}, and Mg^{2+}, *J. Mol. Biol. 264*, 1013−1027.
6. Poland, B. W., Bruns, C., Fromm, H. J., and Honzatko, R. B. (1997) Entrapment of 6-thiophosphoryl-IMP in the active site of crystalline adenylosuccinate synthetase from *Escherichia coli*, *J. Biol. Chem. 272*, 15200−15205.
7. Choe, J. Y., Poland, B. W., Fromm, H. J., and Honzatko, R. B. (1999) Mechanistic implications from crystalline complexes of wild-type and mutant adenylosuccinate synthetases from *Escherichia coli*, *Biochemistry 38*, 6953−6961.
8. Rudolph, F. B., and Fromm, H. J. (1969) Initial rate studies of adenylosuccinate synthetase with product and competitive inhibitors, *J. Biol. Chem. 244*, 3832−3839.
9. Cooper, B. F., Fromm, H. J., and Rudolph, F. B. (1986) Isotope exchange at equilibrium studies with rat muscle adenylosuccinate synthetase, *Biochemistry 25*, 7323−7327.
10. Lowenstein, J. M. (1972) Ammonia production in muscle and other tissues: The purine nucleotide cycle, *Physiol. Rev. 52*, 382−414.
11. Goodman, M. V., and Lowenstein, J. M. (1977) The purine nucleotide cycle. Studies of ammonia production by skeletal muscle *in situ* and in perfused preparations, *J. Biol. Chem. 252*, 5054−5060.
12. Matsuda, Y., Ogawa, H., Fukutome, S., Shiraki, H., and Nakagawa, H. (1977) Adenylosuccinate synthetase in rat liver: The existence of two types and their regulatory roles, *Biochem. Biophys. Res. Commun. 78*, 766−771.
13. Ogawa, H., Shiraki, H., and Nakagawa, H. (1976) Study on the regulatory role of fructose-1,6-diphosphate in the formation of AMP in rat skeletal muscle. A mechanism for synchronization of glycolysis and the purine nucleotide cycle, *Biochem. Biophys. Res. Commun. 68*, 524−528.
14. Guicherit, O. M., Rudolph, F. B., Kellems, R. E., and Cooper, B. F. (1991) Molecular cloning and expression of a mouse muscle cDNA encoding adenylosuccinate synthetase, *J. Biol. Chem. 266*, 22582−22587.
15. Borza, T., Iancu, C. V., Pike, E., Honzatko, R. B., and Fromm, H. J. (2003) Variations in the response of mouse isozymes of adenylosuccinate synthetase to inhibitors of physiological relevance, *J. Biol. Chem. 278*, 6673−6679.
16. Heim, D. R., Cseke, C., Gerwick, B. C., Murdoch, M. G., and Green, S. B. (1995) Hydantocidin: A possible proherbicide inhibiting purine biosynthesis at the site of adenylosuccinate synthetase, *Pestic. Biochem. Physiol. 53*, 138−145.
17. Siehl, D. L., Subramanian, M. V., Walters, E. W., Lee, S.-F., Anderson, R. J., and Toschi, A. G. (1996) Adenylosuccinate synthetase: Site of action of hydantocidin, a microbial phytotoxin, *Plant Physiol. 110*, 753−758.
18. Poland, B. W., Lee, S. F., Subramanian, M. V., Siehl, D. L., Anderson, R. J., Fromm, H. J., and Honzatko, R. B. (1996) Refined crystal structure of adenylosuccinate synthetase from *Escherichia coli* complexed with hydantocidin 5′-phosphate, GDP, HPO_4^{2-}, Mg^{2+}, and hadacidin, *Biochemistry 35*, 15753−15759.
19. Shigeura, H. T., and Gordon, C. N. (1962) The mechanism of action of hadacidin, *J. Biol. Chem. 237*, 1937−1940.
20. Gale, G. R., and Smith, A. B. (1968) Alanosine and hadacidin: Comparison of effects on adenylosuccinate synthetase, *Biochem. Pharmacol. 17*, 2495−2498.
21. Batova, A., Diccianni, M. B., Omura-Minamisawa, M., Yu, J., Carrera, C. J., Bridgeman, L. J., Kung, F. H., Pullen, J., Amylon, M. D., and Yu, A. L. (1999) Use of alanosine as a methylthioadenosine phosphorylase-selective therapy for T-cell acute lymphoblastic leukemia *in vitro*, *Cancer Res. 59*, 1492−1497.

22. Sarma, P. S. A., Mandal, A. K., and Khamis, H. J. (1998) Allopurinol as an additive to quinine in the treatment of acute complicated falciparum malaria, *Am. J. Trop. Med. Hyg. 58*, 454−457.
23. Greenwood, B., and Mutabingwa, T. (2002) Malaria in 2002, *Nature 415*, 670−672.
24. Sachs, J., and Malaney, P. (2002) The economic and social burden of malaria, *Nature 415*, 680−685.
25. Spector, T., Jones, T. E., and Elion, G. B. (1979) Specificity of adenylosuccinate synthetase and adenylosuccinate lyase from *Leishmania donovani*, *J. Biol. Chem. 254*, 8422−8426.
26. Spector, T., Berens, R. L., and Marr, J. J. (1982) Adenylosuccinate synthetase and adenylosuccinate lyase from *Trypanosoma cruzi*, *Biochem. Pharmacol. 31*, 225−229.
27. Iancu, C. V., Borza, T., Fromm, H. J., and Honzatko, R. B. (2002) IMP, GTP, and 6-phosphoryl-IMP complexes of recombinant mouse muscle adenylosuccinate synthetase, *J. Biol. Chem. 277*, 26779−26787.
28. Spector, T., and Miller, R. L. (1976) Mammalian adenylosuccinate synthetase. Nucleotide monophosphate substrates and inhibitors, *Biochim. Biophys. Acta 445*, 509−517.
29. Wang, W., Gorrell, A., Hou, Z., Honzatko, R. B., and Fromm, H. J. (1998) Ambiguities in mapping the active site of a conformationally dynamic enzyme by directed mutation. Role of dynamics in structure-function correlations in *Escherichia coli* adenylosuccinate synthetase, *J. Biol. Chem. 273*, 16000−16004.
30. Iancu, C. V., Borza, T., Choe, J. Y., Fromm, H. J., and Honzatko, R. B. (2001) Recombinant mouse muscle adenylosuccinate synthetase: Overexpression, kinetics, and crystal structure, *J. Biol. Chem. 276*, 42146−42152.
31. Iancu, C. V., Borza, T., Fromm, H. J., and Honzatko, R. B. (2002) Feedback inhibition and product complexes of recombinant mouse-muscle adenylosuccinate synthetase, *J. Biol. Chem. 277*, 40536−40543.
32. Bradford, M. M. (1976) A rapid and sensitive method for the quantitation of microgram quantities of protein utilizing the principle of protein-dye binding, *Anal. Biochem. 72*, 248−254.
33. Leatherbarrow, R. J. (2001) *GraFit*, version 5, Erithacus Software Ltd., Horley, U.K.
34. Otwinowski, Z., and Minor, W. (1997) Processing of X-ray diffraction data collected in oscillation mode, *Methods Enzymol. 276*, 307−326.
35. Hendrixson, T. (2002) *CrystalClear*, version 1.3.5SP2, Rigaku/MSC, Inc., The Woodlands, TX.
36. French, G. S., and Wilson, K. S. (1978) On the treatment of negative intensity observations, *Acta Crystallogr. A34*, 517−525.
37. Navazza, J. (1994) AMoRe: An automated package for molecular replacement, *Acta Crystallogr. A50*, 157−163.
38. McRee, D. E. (1992) *J. Mol. Graphics 10*, 44−46.
39. Brunger, A. T., Adams, P. D., Clore, G. M., DeLano, W. L., Gros, P., Grosse-Kunstleve, R. W., Jiang, J. S., Kuszewski, J., Nilges, M., Pannu, N. S., Read, R. J., Rice, L. M., Simonson, T., and Warren, G. L. (1998) Crystallography & NMR system: A new software suite for macromolecular structure determination, *Acta Crystallogr. D54* (Part 5), 905−921.
40. Engh, R. A., and Huber, R. (1991) Accurate bond and angle parameters for X-ray protein structure refinement, *Acta Crystallogr. A47*, 392−400.
41. Luzzati, V. (1956) *Acta Crystallogr. 5*, 802−810.
42. Laskowski, R. A., MacArthur, M. W., Moss, D. S., and Thornton, J. M. (1993) PROCHECK: A program to check the stereochemical quality of protein structures, *J. Appl. Crystallogr. 26*, 283−291.
43. Collaborative Computational Project, Number 4 (1994) The CCP4 suite: Programs for protein crystallography, *Acta Crystallogr. D50*, 760−763.
44. Goodsell, D. S., and Olson, A. J. (1990) Automated Docking of Substrates to Proteins by Simulated Annealing, *Proteins: Struct., Funct., Genet. 8*, 195−202.
45. Wang, W., Poland, B. W., Honzatko, R. B., and Fromm, H. J. (1995) Identification of arginine residues in the putative L-aspartate binding site of *Escherichia coli* adenylosuccinate synthetase, *J. Biol. Chem. 270*, 13160−13163.
46. Gorrell, A., Wang, W., Underbakke, E., Hou, Z., Honzatko, R. B., and Fromm, H. J. (2002) Determinants of L-aspartate and IMP recognition in *Escherichia coli* adenylosuccinate synthetase, *J. Biol. Chem. 277*, 8817−8821.
47. Fersht, A. R. (1977) Editing mechanisms in protein synthesis. Rejection of valine by isoleucyl-tRNA synthetase, *Biochemistry 16*, 1025−1030.
48. Fersht, A. R., and Dingwall, C. (1979) Establishing the misacylation/deacylation of the tRNA pathway for the editing mechanism of prokaryotic and eukaryotic valyl-tRNA synthases, *Biochemistry 18*, 1238−1245.
49. Fersht, A. R., Shindler, J. S., and Tsui, W.-C. (1980) Probing the limits of protein-amino acid side chain recognition with aminoacyl-tRNA synthetases. Discrimination against phenylalanine by tyrosyl-tRNA synthetases, *Biochemistry 19*, 5520−5524.
50. Fersht, A. R., and Dingwall, C. (1979) Cysteinyl-tRNA synthetase from *Escherichia coli* does not need an editing mechanism to reject serine and alanine. High binding energy of small groups in specific molecular interactions, *Biochemistry 18*, 1245−1249.
51. Musk, P., Clark, J. M., Thompson, D., Dunn, I. S., Christopherson, R. I., Szabados, E., Rose, S. E., and Parsons, P. G. (1996) Purine deoxynucleoside metabolism in human melanoma cells with high spontaneous mutation rate, *Mutat. Res. 350*, 229−238.
52. Markham, G. D., Bock, C. L., and Schalk-Hihi, C. (1999) Acid-base catalysis in the chemical mechanism of inosine monophosphate dehydrogenase, *Biochemistry 38*, 4433−4440.
53. Zheng, R., and Blanchard, J. S. (2001) Steady-state and pre-steady-state kinetic analysis of *Mycobacterium tuberculosis* pantothenate synthetase, *Biochemistry 40*, 12904−12912.
54. Wang, S., and Eisenberg, D. (2006) Crystal structure of the pantothenate synthetase from *Mycobacterium tuberculosis*, snapshots of the enzyme in action, *Biochemistry 45*, 1554−1561.
55. Thoden, J. B., Firestine, S., Nixon, A., Benkovic, S. J., and Holden, H. M. (2000) Molecular structure of *Escherichia coli* purT-encoded glycinamide ribonucleotide transformylase, *Biochemistry 39*, 8791−8802.
56. Lindstrom, W. N., Jr., Flynn, J., and Reich, N. O. (2000) Reconciling structure and function in *Hha*I DNA cytosine-C-5 methyltransferase, *J. Biol. Chem. 275*, 4912−4919.
57. Kraulis, J. (1991) MOLSCRIPT: A program to produce both detailed and schematic plots of protein structures, *J. Appl. Crystallogr. 24*, 946−950.
58. DeLeno, W. L. (2002) *The PyMOL molecular graphics system*, DeLano Scientific, San Carlos, CA.

BI0607498